



This is the accepted manuscript made available via CHORUS. The article has been published as:

Azimuthal anisotropy measurement of (multi)strange
hadrons in Au+Au collisions at $\sqrt{s_{NN}} = 54.4$
GeV

M. S. Abdallah et al. (STAR Collaboration)

Phys. Rev. C **107**, 024912 — Published 22 February 2023

DOI: [10.1103/PhysRevC.107.024912](https://doi.org/10.1103/PhysRevC.107.024912)

1 **Azimuthal anisotropy measurement of (multi-)strange hadrons in Au+Au collisions at**
2 $\sqrt{s_{NN}} = 54.4$ GeV

3 M. S. Abdallah,¹ B. E. Aboona,² J. Adam,³ L. Adamczyk,⁴ J. R. Adams,⁵ J. K. Adkins,⁶ I. Aggarwal,⁷
4 M. M. Aggarwal,⁷ Z. Ahammed,⁸ D. M. Anderson,² E. C. Aschenauer,³ J. Atchison,⁹ V. Bairathi,¹⁰ W. Baker,¹¹
5 J. G. Ball Cap,¹² K. Barish,¹¹ R. Bellwied,¹² P. Bhagat,¹³ A. Bhasin,¹³ S. Bhatta,¹⁴ J. Bielcik,¹⁵ J. Bielcikova,¹⁶
6 J. D. Brandenburg,³ X. Z. Cai,¹⁷ H. Caines,¹⁸ M. Calderón de la Barca Sánchez,¹⁹ D. Cebra,¹⁹ I. Chakaberia,²⁰
7 P. Chaloupka,¹⁵ B. K. Chan,²¹ Z. Chang,²² A. Chatterjee,²³ S. Chattopadhyay,⁸ D. Chen,¹¹ J. Chen,²⁴
8 J. H. Chen,²⁵ X. Chen,²⁶ Z. Chen,²⁴ J. Cheng,²⁷ S. Choudhury,²⁵ W. Christie,³ X. Chu,³ H. J. Crawford,²⁸
9 M. Csanád,²⁹ M. Daugherty,⁹ I. M. Deppner,³⁰ A. Dhamija,⁷ L. Di Carlo,³¹ L. Didenko,³ P. Dixit,³² X. Dong,²⁰
10 J. L. Drachenberg,⁹ E. Duckworth,³³ J. C. Dunlop,³ J. Engelage,²⁸ G. Eppley,³⁴ S. Esumi,³⁵ O. Evdokimov,³⁶
11 A. Ewigleben,³⁷ O. Eyser,³ R. Fatemi,⁶ F. M. Fawzi,¹ S. Fazio,³⁸ C. J. Feng,³⁹ Y. Feng,⁴⁰ E. Finch,⁴¹ Y. Fisyak,³
12 A. Francisco,¹⁸ C. Fu,⁴² C. A. Gagliardi,² T. Galatyuk,⁴³ F. Geurts,³⁴ N. Ghimire,⁴⁴ A. Gibson,⁴⁵ K. Gopal,⁴⁶
13 X. Gou,²⁴ D. Grosnick,⁴⁵ A. Gupta,¹³ W. Guryn,³ A. Hamed,¹ Y. Han,³⁴ S. Harabasz,⁴³ M. D. Harasty,¹⁹
14 J. W. Harris,¹⁸ H. Harrison,⁶ S. He,⁴² W. He,²⁵ X. H. He,⁴⁷ Y. He,²⁴ S. Heppelmann,¹⁹ N. Herrmann,³⁰
15 E. Hoffman,¹² L. Holub,¹⁵ C. Hu,⁴⁷ Q. Hu,⁴⁷ Y. Hu,²⁰ H. Huang,³⁹ H. Z. Huang,²¹ S. L. Huang,¹⁴ T. Huang,³⁹
16 X. Huang,²⁷ Y. Huang,²⁷ T. J. Humanic,⁵ D. Isenhower,⁹ M. Isshiki,³⁵ W. W. Jacobs,²² C. Jena,⁴⁶
17 A. Jentsch,³ Y. Ji,²⁰ J. Jia,^{3,14} K. Jiang,²⁶ C. Jin,³⁴ X. Ju,²⁶ E. G. Judd,²⁸ S. Kabana,¹⁰ M. L. Kabir,¹¹
18 S. Kagamaster,³⁷ D. Kalinkin,^{22,3} K. Kang,²⁷ D. Kapukchyan,¹¹ K. Kauder,³ H. W. Ke,³ D. Keane,³³ M. Kelsey,³¹
19 Y. V. Khyzhniak,⁵ D. P. Kikoła,²³ B. Kimelman,¹⁹ D. Kincses,²⁹ I. Kisel,⁴⁸ A. Kiselev,³ A. G. Knospe,³⁷
20 H. S. Ko,²⁰ L. K. Kosarzewski,¹⁵ L. Kramerik,¹⁵ L. Kumar,⁷ S. Kumar,⁴⁷ R. Kunnawalkam Elayavalli,¹⁸
21 J. H. Kwasizur,²² R. Lacey,¹⁴ S. Lan,⁴² J. M. Landgraf,³ J. Lauret,³ A. Lebedev,³ J. H. Lee,³ Y. H. Leung,²⁰
22 N. Lewis,³ C. Li,²⁴ C. Li,²⁶ W. Li,³⁴ W. Li,¹⁷ X. Li,²⁶ Y. Li,²⁶ Y. Li,²⁷ Z. Li,²⁶ X. Liang,¹¹ Y. Liang,³³
23 R. Licensik,^{16,15} T. Lin,²⁴ Y. Lin,⁴² M. A. Lisa,⁵ F. Liu,⁴² H. Liu,²² H. Liu,⁴² T. Liu,¹⁸ X. Liu,⁵ Y. Liu,²
24 T. Ljubicic,³ W. J. Llope,³¹ R. S. Longacre,³ E. Loyd,¹¹ T. Lu,⁴⁷ N. S. Lukow,⁴⁴ X. F. Luo,⁴² L. Ma,²⁵ R. Ma,³
25 Y. G. Ma,²⁵ N. Magdy,³⁶ D. Mallick,⁴⁹ S. Margetis,³³ C. Markert,⁵⁰ H. S. Matis,²⁰ J. A. Mazer,⁵¹ G. McNamara,³¹
26 S. Mioduszewski,² B. Mohanty,⁴⁹ M. M. Mondal,⁴⁹ I. Mooney,¹⁸ A. Mukherjee,²⁹ M. I. Nagy,²⁹ A. S. Nain,⁷
27 J. D. Nam,⁴⁴ Md. Nasim,³² K. Nayak,⁴⁶ D. Neff,²¹ J. M. Nelson,²⁸ D. B. Nemes,¹⁸ M. Nie,²⁴ T. Niida,³⁵
28 R. Nishitani,³⁵ T. Nonaka,³⁵ A. S. Nunes,³ G. Odyniec,²⁰ A. Ogawa,³ S. Oh,²⁰ K. Okubo,³⁵ B. S. Page,³ R. Pak,³
29 J. Pan,² A. Pandav,⁴⁹ A. K. Pandey,³⁵ A. Paul,¹¹ B. Pawlik,⁵² D. Pawlowska,²³ C. Perkins,²⁸ J. Pluta,²³
30 B. R. Pokhrel,⁴⁴ J. Porter,²⁰ M. Posik,⁴⁴ V. Prozorova,¹⁵ N. K. Pruthi,⁷ M. Przybycien,⁴ J. Putschke,³¹
31 Z. Qin,²⁷ H. Qiu,⁴⁷ A. Quintero,⁴⁴ C. Racz,¹¹ S. K. Radhakrishnan,³³ N. Raha,³¹ R. L. Ray,⁵⁰ R. Reed,³⁷
32 H. G. Ritter,²⁰ M. Robotkova,^{16,15} J. L. Romero,¹⁹ D. Roy,⁵¹ P. Roy Chowdhury,²³ L. Ruan,³ A. K. Sahoo,³²
33 N. R. Sahoo,²⁴ H. Sako,³⁵ S. Salur,⁵¹ S. Sato,³⁵ W. B. Schmidke,³ N. Schmitz,⁵³ F.-J. Seck,⁴³ J. Seger,⁵⁴
34 M. Sergeeva,²¹ R. Seto,¹¹ P. Seyboth,⁵³ N. Shah,⁵⁵ P. V. Shanmuganathan,³ M. Shao,²⁶ T. Shao,²⁵ R. Sharma,⁴⁶
35 A. I. Sheikh,³³ D. Y. Shen,²⁵ K. Shen,²⁶ S. S. Shi,⁴² Y. Shi,²⁴ Q. Y. Shou,²⁵ E. P. Sichtermann,²⁰ R. Sikora,⁴
36 J. Singh,⁷ S. Singha,⁴⁷ P. Sinha,⁴⁶ M. J. Skoby,^{56,40} N. Smirnov,¹⁸ Y. Söhngen,³⁰ W. Solyst,²² Y. Song,¹⁸
37 B. Srivastava,⁴⁰ T. D. S. Stanislaus,⁴⁵ M. Stefaniak,²³ D. J. Stewart,³¹ B. Stringfellow,⁴⁰ A. A. P. Suaide,⁵⁷
38 M. Sumbera,¹⁶ C. Sun,¹⁴ X. M. Sun,⁴² X. Sun,⁴⁷ Y. Sun,²⁶ Y. Sun,⁵⁸ B. Surrow,⁴⁴ Z. W. Sweger,¹⁹ P. Szymanski,²³
39 A. H. Tang,³ Z. Tang,²⁶ T. Tarnowsky,⁵⁹ J. H. Thomas,²⁰ A. R. Timmins,¹² D. Tlusty,⁵⁴ T. Todoroki,³⁵
40 C. A. Tomkiel,³⁷ S. Trentalange,²¹ R. E. Tribble,² P. Tribedy,³ S. K. Tripathy,²⁹ T. Truhlar,¹⁵ B. A. Trzeciak,¹⁵
41 O. D. Tsai,²¹ C. Y. Tsang,^{33,3} Z. Tu,³ T. Ullrich,³ D. G. Underwood,^{60,45} I. Upsal,³⁴ G. Van Buren,³ J. Vanek,^{3,15}
42 I. Vassiliev,⁴⁸ V. Verkest,³¹ F. Videbæk,³ S. A. Voloshin,³¹ F. Wang,⁴⁰ G. Wang,²¹ J. S. Wang,⁵⁸ P. Wang,²⁶
43 X. Wang,²⁴ Y. Wang,⁴² Y. Wang,²⁷ Z. Wang,²⁴ J. C. Webb,³ P. C. Weidenkaff,³⁰ G. D. Westfall,⁵⁹ D. Wielanek,²³
44 H. Wieman,²⁰ S. W. Wissink,²² R. Witt,⁶¹ J. Wu,⁴² J. Wu,⁴⁷ Y. Wu,¹¹ B. Xi,¹⁷ Z. G. Xiao,²⁷ G. Xie,²⁰ W. Xie,⁴⁰
45 H. Xu,⁵⁸ N. Xu,²⁰ Q. H. Xu,²⁴ Y. Xu,²⁴ Z. Xu,³ Z. Xu,²¹ G. Yan,²⁴ Z. Yan,¹⁴ C. Yang,²⁴ Q. Yang,²⁴ S. Yang,⁶²
46 Y. Yang,³⁹ Z. Ye,³⁴ Z. Ye,³⁶ L. Yi,²⁴ K. Yip,³ Y. Yu,²⁴ H. Zbroszczyk,²³ W. Zha,²⁶ C. Zhang,¹⁴ D. Zhang,⁴²
47 J. Zhang,²⁴ S. Zhang,²⁶ S. Zhang,²⁵ Y. Zhang,⁴⁷ Y. Zhang,²⁶ Y. Zhang,⁴² Z. J. Zhang,³⁹ Z. Zhang,³ Z. Zhang,³⁶
48 F. Zhao,⁴⁷ J. Zhao,²⁵ M. Zhao,³ C. Zhou,²⁵ J. Zhou,²⁶ Y. Zhou,⁴² X. Zhu,²⁷ M. Zurek,⁶⁰ and M. Zyzak⁴⁸

49 (STAR Collaboration)

50 ¹American University of Cairo, New Cairo 11835, New Cairo, Egypt

51 ²Texas A&M University, College Station, Texas 77843

52 ³Brookhaven National Laboratory, Upton, New York 11973

53 ⁴AGH University of Science and Technology, FPACS, Cracow 30-059, Poland

- 54 ⁵Ohio State University, Columbus, Ohio 43210
55 ⁶University of Kentucky, Lexington, Kentucky 40506-0055
56 ⁷Panjab University, Chandigarh 160014, India
57 ⁸Variable Energy Cyclotron Centre, Kolkata 700064, India
58 ⁹Abilene Christian University, Abilene, Texas 79699
59 ¹⁰Instituto de Alta Investigación, Universidad de Tarapacá, Arica 1000000, Chile
60 ¹¹University of California, Riverside, California 92521
61 ¹²University of Houston, Houston, Texas 77204
62 ¹³University of Jammu, Jammu 180001, India
63 ¹⁴State University of New York, Stony Brook, New York 11794
64 ¹⁵Czech Technical University in Prague, FNSPE, Prague 115 19, Czech Republic
65 ¹⁶Nuclear Physics Institute of the CAS, Rez 250 68, Czech Republic
66 ¹⁷Shanghai Institute of Applied Physics, Chinese Academy of Sciences, Shanghai 201800
67 ¹⁸Yale University, New Haven, Connecticut 06520
68 ¹⁹University of California, Davis, California 95616
69 ²⁰Lawrence Berkeley National Laboratory, Berkeley, California 94720
70 ²¹University of California, Los Angeles, California 90095
71 ²²Indiana University, Bloomington, Indiana 47408
72 ²³Warsaw University of Technology, Warsaw 00-661, Poland
73 ²⁴Shandong University, Qingdao, Shandong 266237
74 ²⁵Fudan University, Shanghai, 200433
75 ²⁶University of Science and Technology of China, Hefei, Anhui 230026
76 ²⁷Tsinghua University, Beijing 100084
77 ²⁸University of California, Berkeley, California 94720
78 ²⁹ELTE Eötvös Loránd University, Budapest, Hungary H-1117
79 ³⁰University of Heidelberg, Heidelberg 69120, Germany
80 ³¹Wayne State University, Detroit, Michigan 48201
81 ³²Indian Institute of Science Education and Research (IISER), Berhampur 760010, India
82 ³³Kent State University, Kent, Ohio 44242
83 ³⁴Rice University, Houston, Texas 77251
84 ³⁵University of Tsukuba, Tsukuba, Ibaraki 305-8571, Japan
85 ³⁶University of Illinois at Chicago, Chicago, Illinois 60607
86 ³⁷Lehigh University, Bethlehem, Pennsylvania 18015
87 ³⁸University of Calabria & INFN-Cosenza, Italy
88 ³⁹National Cheng Kung University, Tainan 70101
89 ⁴⁰Purdue University, West Lafayette, Indiana 47907
90 ⁴¹Southern Connecticut State University, New Haven, Connecticut 06515
91 ⁴²Central China Normal University, Wuhan, Hubei 430079
92 ⁴³Technische Universität Darmstadt, Darmstadt 64289, Germany
93 ⁴⁴Temple University, Philadelphia, Pennsylvania 19122
94 ⁴⁵Valparaiso University, Valparaiso, Indiana 46383
95 ⁴⁶Indian Institute of Science Education and Research (IISER) Tirupati, Tirupati 517507, India
96 ⁴⁷Institute of Modern Physics, Chinese Academy of Sciences, Lanzhou, Gansu 730000
97 ⁴⁸Frankfurt Institute for Advanced Studies FIAS, Frankfurt 60438, Germany
98 ⁴⁹National Institute of Science Education and Research, HBNI, Jatni 752050, India
99 ⁵⁰University of Texas, Austin, Texas 78712
100 ⁵¹Rutgers University, Piscataway, New Jersey 08854
101 ⁵²Institute of Nuclear Physics PAN, Cracow 31-342, Poland
102 ⁵³Max-Planck-Institut für Physik, Munich 80805, Germany
103 ⁵⁴Creighton University, Omaha, Nebraska 68178
104 ⁵⁵Indian Institute Technology, Patna, Bihar 801106, India
105 ⁵⁶Ball State University, Muncie, Indiana, 47306
106 ⁵⁷Universidade de São Paulo, São Paulo, Brazil 05314-970
107 ⁵⁸Huzhou University, Huzhou, Zhejiang 313000
108 ⁵⁹Michigan State University, East Lansing, Michigan 48824
109 ⁶⁰Argonne National Laboratory, Argonne, Illinois 60439
110 ⁶¹United States Naval Academy, Annapolis, Maryland 21402
111 ⁶²South China Normal University, Guangzhou, Guangdong 510631

112 Azimuthal anisotropy of produced particles is one of the most important observables used to
113 access the collective properties of the expanding medium created in relativistic heavy-ion collisions.
114 In this paper, we present second (v_2) and third (v_3) order azimuthal anisotropies of K_S^0 , ϕ , Λ , Ξ
115 and Ω at mid-rapidity ($|y| < 1$) in Au+Au collisions at $\sqrt{s_{NN}} = 54.4$ GeV measured by the STAR
116 detector. The v_2 and v_3 are measured as a function of transverse momentum and centrality. Their

energy dependence is also studied. v_3 is found to be more sensitive to the change in the center-of-mass energy than v_2 . Scaling by constituent quark number is found to hold for v_2 within 10%. This observation could be evidence for the development of partonic collectivity in 54.4 GeV Au+Au collisions. Differences in v_2 and v_3 between baryons and anti-baryons are presented, and ratios of $v_3/v_2^{3/2}$ are studied and motivated by hydrodynamical calculations. The ratio of v_2 of ϕ mesons to that of anti-protons ($v_2(\phi)/v_2(\bar{p})$) shows centrality dependence at low transverse momentum, presumably resulting from the larger effects from hadronic interactions on anti-proton v_2 .

I. INTRODUCTION

According to Quantum ChromoDynamics (QCD), at very high temperature (T) and/or large baryonic chemical potential (μ_B) a deconfined phase of quarks and gluons is expected to be present, while at low T and low μ_B quarks and gluons are known to be confined inside hadrons [1]. High energy heavy-ion collisions provide a unique opportunity to study QCD matter at extremely high temperature and density. Experiments at the Relativistic Heavy Ion Collider (RHIC) have shown that a very dense medium of deconfined quarks and gluons is formed in Au+Au collisions at the center-of-mass energy of $\sqrt{s_{NN}} = 200$ GeV [2–9]. Azimuthal anisotropy parameters (v_n), which quantify the azimuthal asymmetries of particle production in momentum space, are an excellent tool to study the properties of the deconfined medium created in these collisions [10–17]. Observations of large v_n magnitudes and their constituent quark scaling in 200 GeV Au+Au collisions ($\mu_B \sim 20$ MeV) have been considered a signature of partonic collectivity of the system [18].

To study the QCD phase structure over a large range in T and μ_B , a beam energy scan program has been carried out by RHIC. The first phase of this program (BES-I) was carried out in 2010-14. Measurements of azimuthal anisotropies of light flavor hadrons made during during the BES-I program by the STAR experiment indicate the formation of QCD matter dominated by hadronic interactions in Au+Au collisions at $\sqrt{s_{NN}} < 11.5$ GeV ($\mu_B > 200$ MeV) [20, 21].

Strange hadrons, especially those containing more than one strange quark, are considered a good probe to study the collective properties of the medium created in the early stage of heavy-ion collisions [2, 22–26]. The measurement of average transverse momentum $\langle p_T \rangle$ of ϕ mesons shows weak centrality dependence while $\langle p_T \rangle$ of protons increases significantly from peripheral to central collisions. This could be due to the fact that ϕ mesons have relatively small hadronic interaction cross-section compared to that of proton [27]. Measurements of (multi-)strange hadron v_n is limited by the available statistics in BES-I. In this paper, we report high precision measurements of azimuthal anisotropy parameters, v_2 and v_3 , of strange and multi-strange hadrons at mid-rapidity ($|y| < 1$) in Au+Au collisions at $\sqrt{s_{NN}} = 54.4$ GeV ($\mu_B \sim 90$ MeV). v_2 and v_3 of K_S^0 , ϕ , Λ , Ξ and Ω are measured as a function of particle transverse momentum (p_T) and collision centrality. Such measurements will provide deep insights into properties of the hot and dense medium, such as partonic collectivity, transport coefficients, and

hadronization mechanisms.

This paper is organized in the following manner. In sections II, III and IV, we describe the dataset, the analysis method, and systematic studies respectively. In section V we report the results. Finally, a summary is given in section VI.

II. EXPERIMENTAL SETUP

In this analysis, a total of 600 M minimum bias Au+Au events at $\sqrt{s_{NN}} = 54.4$ GeV recorded by the STAR experiment are used. Events for analysis are selected based on the collision vertex position. Along the beam direction, a vertex position cut of $|V_z| < 30$ cm is applied. A radial vertex position cut (defined as $V_r = \sqrt{V_x^2 + V_y^2}$) of $V_r < 2.0$ cm is used in order to avoid collision with beam pipe whose radius is 3.95 cm.

The trajectory of a charged particle through STARs magnetic field can be reconstructed, and thus its momentum determined, using the Time Projection Chamber (TPC) [28]. To ensure good track quality, the number of TPC hit points on each track is required to be larger than 15, and the ratio of the number of used TPC hit points to the maximum possible number of hit points along the trajectory should be larger than 0.52. The transverse momentum of each particle is limited to $p_T > 0.15$ GeV/c.

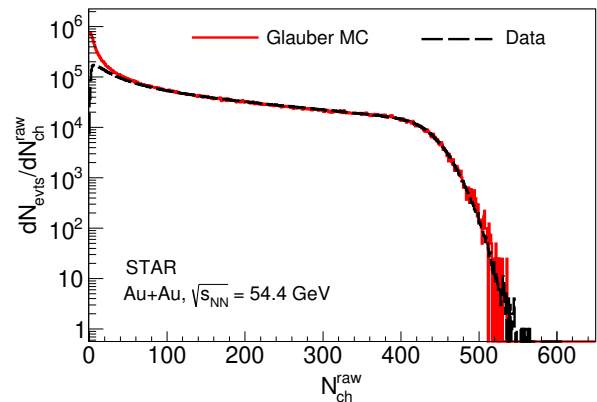


FIG. 1. The uncorrected multiplicity distribution of reconstructed charged particles in Au+Au collisions at $\sqrt{s_{NN}} = 54.4$ GeV. Glauber Monte Carlo simulation is shown as the solid red curve.

The collision centrality is determined by comparing the

uncorrected charged particle multiplicity within a pseudorapidity range of $|\eta| < 0.5$ measured by the TPC with a Glauber Monte Carlo (MC) [29] simulation as shown in Fig. 1. The significant difference between the measured multiplicity and Glauber simulation at low multiplicity values is due to trigger and primary vertex finding inefficiency. This is corrected by taking the ratio of the simulated multiplicity distribution to that in data as a weight factor. The detailed procedure to obtain the simulated multiplicity distribution using Glauber MC is similar to that described in Ref. [30]. Central (peripheral) events correspond to collisions of large (small) nuclear overlap and thus large (small) charged particle multiplicities.

Particle identification is done using the TPC and the Time-of-Flight (TOF) detectors [31] at mid-pseudorapidity ($|\eta| < 1.0$). Both the TPC and TOF have full azimuth coverage. Long-lived charged particles, e.g. π , K , and p , are identified directly using specific ionization energy loss in the TPC and time of flight information in TOF [21]. Short-lived strange hadrons (K_S^0 , ϕ , Λ , Ξ , Ω) are reconstructed through two-body hadronic decay channels: $K_S^0 \rightarrow \pi^+ + \pi^-$, $\phi \rightarrow K^+ + K^-$, $\Lambda(\bar{\Lambda}) \rightarrow p(\bar{p}) + \pi^-(\pi^+)$, $\Xi^\pm \rightarrow \Lambda + \pi^\pm$ and $\Omega^\pm \rightarrow \Lambda + K^\pm$. K_S^0 , Λ , Ξ , and Ω decay weakly and therefore decay topology cuts are applied to reduce the combinatorial background. Cuts on the following topological variables are used: (1) Distance of Closest Approach (DCA) between the two daughter tracks, (2) the DCA of the daughter tracks to the collision vertex, (3) the DCA of the reconstructed parent strange hadron to the collision vertex, (4) the decay length of the strange hadrons, and (5) the angle between the spatial vector pointing from the collision vertex to the decay vertex and the momentum vector of the parent strange hadron. Since the ϕ meson decays strongly, its daughter kaons appear to originate from the collision vertex. The DCAs of kaon tracks from the collision vertex are required to be less than 3 cm for ϕ meson reconstruction.

An event mixing technique is used for the subtraction of combinatorial background for the ϕ mesons [32] and different polynomial functions (1st and 2nd order) are used to fit the background after mixed-event background subtraction. For K_S^0 and Λ , the like-sign method is used to estimate the background and for Ξ and Ω , the rotational background method is used [33–35]. The invariant mass distributions of K_S^0 , ϕ , Λ , Ξ^- , Ω^- and their anti-particles are shown in Fig. 2. The invariant mass distribution for Ξ^- (Ξ^+) has a small bump due to the combinatorial Λ background [33].

III. ANALYSIS METHOD

The n^{th} order flow coefficient with respect to the event plane is given by

$$v_n = \frac{\langle \cos n(\Phi_i - \psi_n) \rangle}{R_n}, \quad (1)$$

where the angle-bracket represents the average over all the particles in each event and over all the events, Φ_i is the azimuthal angle of the i^{th} particle in an event and ψ_n is the event plane angle for the n^{th} order anisotropy of an event [36]. The R_n denotes the resolution of the n^{th} order event plane angle. The event plane angle can be determined based on the azimuthal distribution of particles in the plane transverse to the collision axis. The n^{th} order event plane angle is given by

$$\psi_n = \frac{1}{n} \tan^{-1} \frac{\sum_i w_i \sin(n\Phi_i)}{\sum_i w_i \cos(n\Phi_i)}. \quad (2)$$

Here w_i is the weight factor taken as p_T of the particle for optimal resolution. The n^{th} order event plane has a symmetry of $2\pi/n$ and one would expect an isotropic distribution of the event plane angle from 0 to $2\pi/n$. However, due to the azimuthally non-uniform detection efficiency of the TPC, the reconstructed event plane angle distribution is usually not isotropic. This is corrected for using the Φ -weight method, details of which can be found in the ref. [36].

To suppress the auto-correlation between particles of interest and those used for event plane angle determination [30, 36], calculations of the v_n coefficients for particles in the positive pseudorapidity region ($0 < \eta < 1$) utilize the sub-event plane determined using particles in the negative pseudorapidity region ($-1 < \eta < -0.05$), and vice versa. Its definition is the following:

$$v_n = \frac{\langle \cos n(\Phi_i - \psi_n^{A/B}) \rangle}{R_n}, \quad (3)$$

where ψ_n^A and ψ_n^B are the sub-event planes in negative ($-1 < \eta < -0.05$) and positive ($0.05 < \eta < 1$) pseudorapidity regions, respectively. In addition to that, auto-correlation has been removed in the case when decay daughters are distributed in sub-events.

The event plane resolution R_n is estimated using:

$$R_n = \langle \cos n(\psi_n - \psi_R) \rangle = \sqrt{\langle \cos n(\psi_n^A - \psi_n^B) \rangle}, \quad (4)$$

in which ψ_R is the reaction plane angle. Resolution corrections for wide centrality bins are done using the method described in Ref. [37]. ψ_2 and ψ_3 resolution in different centrality bins are given in Table I

By using equation 3, one can calculate the v_n of particles that are detected directly and whose azimuthal distributions are known in every event. But the particles used in this analysis are short-lived and can't be detected directly. To calculate the v_n of such particles, the invariant mass method is used [38], in which the v_n of the particle of interest is calculated as a function of the invariant mass of the decayed daughter particles. Figure 3, taking K_S^0 as an example, shows v_2 and v_3 as a function of the $\pi^+\pi^-$ pair invariant mass in the 10-40% centrality bin. The total v_n of the signal+background can be decomposed into two parts.

$$v_n^{S+B} = v_n^S \frac{S}{S+B} + v_n^B \frac{B}{S+B}. \quad (5)$$

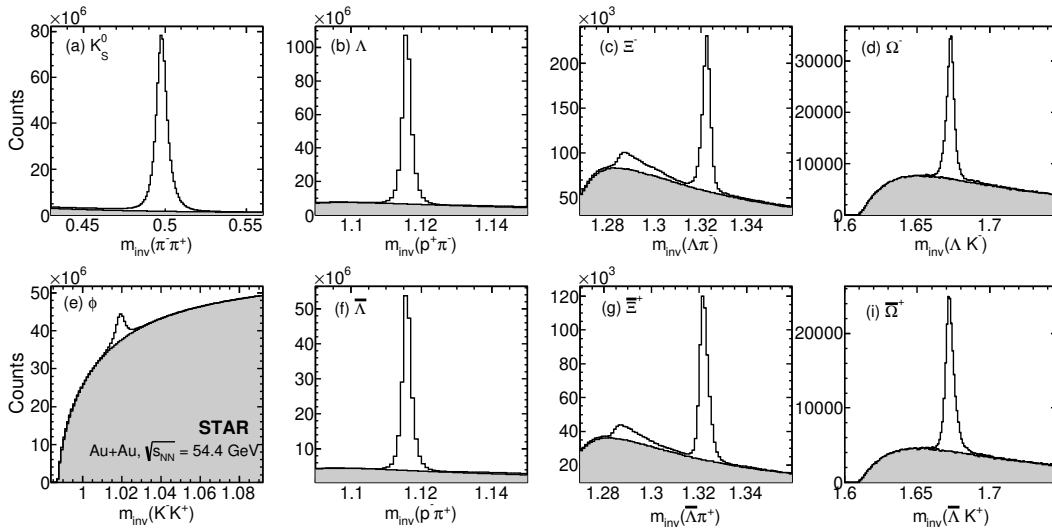


FIG. 2. Invariant mass distributions for K_S^0 , ϕ , Λ , Ξ^- , Ω^- and their anti-particles in minimum bias Au+Au collisions at $\sqrt{s_{NN}} = 54.4$ GeV. The combinatorial background is shown as gray shaded histograms. No background subtraction was included in any of the 8 panels.

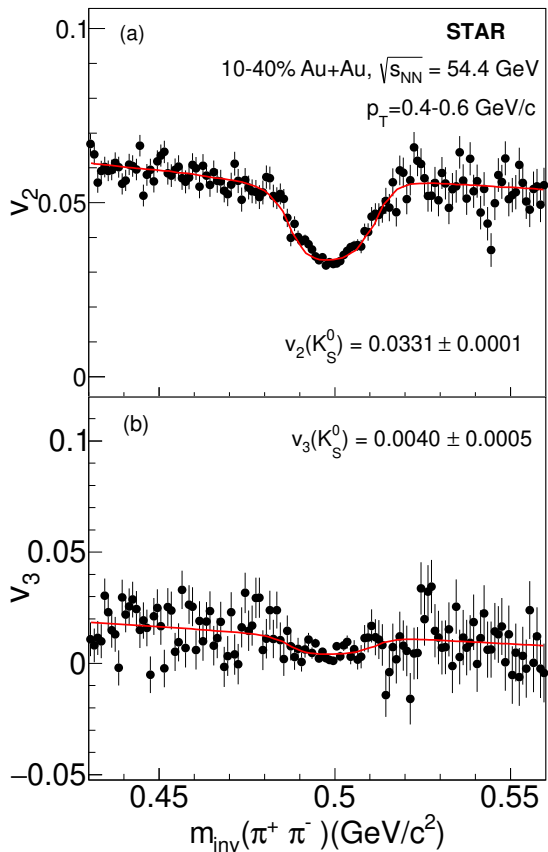


FIG. 3. The upper panel shows v_2 as a function of the invariant mass of $\pi^+ \pi^-$ pairs and the lower panel shows the same for v_3 . Red lines represent fit functions given in Eq. 5

Centrality	ψ_2 resolution	ψ_3 resolution
0-5%	0.3462 ± 0.0002	0.2284 ± 0.0003
5-10%	0.4549 ± 0.0001	0.2360 ± 0.0002
10-20%	0.54179 ± 0.00007	0.2257 ± 0.0002
20-30%	0.56211 ± 0.00007	0.1981 ± 0.0002
30-40%	0.51865 ± 0.00008	0.1636 ± 0.0003
40-50%	0.4338 ± 0.0001	0.1234 ± 0.0003
50-60%	0.3289 ± 0.0001	0.0863 ± 0.0005
60-70%	0.2295 ± 0.0002	0.0564 ± 0.0008
70-80%	0.1578 ± 0.0003	0.028 ± 0.002

TABLE I. Resolution for ψ_2 and ψ_3 in different centrality bins.

302 Here v_n^S is the v_n of the signal (K_S^0), v_n^B is the v_n of
 303 the background, S is the raw signal counts and B is the
 304 background counts. v_n^B is approximated with a first order
 305 polynomial function. v_n^S is a free parameter and can be
 306 obtained by fitting v_n using Eq. 5, shown as solid red
 307 lines in Fig. 3. The v_2 and v_3 of other strange hadrons
 308 are calculated in a similar way except for Ξ . For Ξ , Eq. 5
 309 has been modified as follows:

$$v_n^{S+B} = v_n^S \frac{S}{S+B+b} + v_n^b \frac{b}{S+B+b} + v_n^B \frac{B}{S+B+b}, \quad (6)$$

310 where b denotes the yield of the residual bump observed
 311 in the low invariant mass region (see Fig. 2), and v_n^b de-
 312 notes the v_n of the residual candidates in the bump re-
 313 gion. Systematic checks have been carried out to examine
 314 the effect of the bump in Ξ v_n extraction by changing fit
 315 ranges and the shape of the background v_n^b at the bump
 316 region. The effect is found to be negligibly small, less
 317 than 1%, on the v_n values of Ξ particles.

Particle/Centrality	0-10%	10-40%	40-80%	0-80%
K_S^0	2%	2%	2%	2%
ϕ	10%	3%	3%	5%
Λ	2%	2%	2%	2%
Ξ	4%	3%	3%	3%
Ω	22%	6%	15%	8%

TABLE II. Average systematic uncertainties on v_2 of K_S^0 , ϕ , Λ , Ξ and Ω in different centrality bins.

Particle/Centrality	0-10%	10-40%	40-80%	0-80%
K_S^0	3%	3%	3%	3%
ϕ	15%	10%	N.A.	10%
Λ	3%	3%	3%	3%
Ξ	12%	10%	N.A.	8%
Ω	30%	30%	N.A.	30%

TABLE III. Average systematic uncertainties on v_3 of K_S^0 , ϕ , Λ , Ξ and Ω in different centrality bins.

IV. SYSTEMATIC UNCERTAINTY

Systematic uncertainties are evaluated by varying event selection cuts, track selection cuts, and background subtraction methods. Track selection cuts used for event plane angle calculation are also varied. For particles like Ξ and Ω the default background construction method is the rotational method and for particles like K_S^0 and Λ the default background construction method is the like-sign method. As an alternative to estimate the background fraction, polynomial functions are used to model the residual background in fitting the invariant mass distributions. The resulting differences in v_n between using the default and alternative background estimation methods are included in the systematic uncertainties. For weakly decaying particles, topological cuts are varied as well. Different topological variables are varied simultaneously to keep the raw yield of the particle of interest similar. This helps to reduce the effect of statistical fluctuations in estimating systematic uncertainties. Finally, the Barlow's method [39] is used to determine the systematic uncertainties arising from analysis cut variations. If the resulting changes (Δv_n) in v_n are smaller than the change in statistical errors ($\Delta\sigma_{stat}$) on v_n , such changes are not included in the uncertainties. Otherwise, the systematic error (σ_{sys}) on v_n is calculated as $\sigma_{sys} = \sqrt{(\Delta v_n)^2 - (\Delta\sigma_{stat})^2}$. Finally, systematic uncertainties from different sources, which pass the Barlow check, are added in quadrature. Final systematic uncertainties are calculated as a function of p_T and centrality. They are found to be nearly p_T independent but larger in central collisions compared to peripheral collisions. Table II and III show the average systematic uncertainties on v_2 and v_3 for K_S^0 , ϕ , Λ , Ξ and Ω in different centrality bins.

V. RESULTS AND DISCUSSION

A. p_T dependence of v_2 and v_3

The transverse momentum dependence of v_2 and v_3 for K_S^0 , ϕ , Λ , Ξ^- , Ω^- (and their anti-particles) is shown in Fig. 4. The measurements are done at mid-rapidity, $|y| < 1.0$, in minimum bias Au+Au collisions at $\sqrt{s_{NN}} = 54.4$ GeV. The non-zero magnitude of v_3 is consistent with the picture of event-by-event fluctuations in the initial density profile of the colliding nuclei [40]. Both v_2 and v_3 initially increase with p_T and then tend to saturate. This may be due to the interplay of hydrodynamic flow as well as viscous effects [41]. The magnitude of v_3 is found to be less than that of v_2 for all particles in 0-80% centrality. This is the first v_3 measurement of the multi-strange baryons Ξ and Ω in relativistic heavy-ion collisions. The v_n of heavy multi-strange baryons like Ω are similar to that of the lighter mass, strange baryon Λ . The v_n of ϕ mesons, which consist of strange and anti-strange quark pairs, is similar to that of light, strange K_S^0 . If v_n is developed through hadronic interactions, v_n should depend on the cross-sections of the interacting hadrons and therefore those (e.g. ϕ , Ω) with smaller cross-sections should develop less momentum anisotropy. Therefore the observed large v_n of ϕ and Ω are consistent with the scenario that the anisotropy is developed in the partonic medium in Au+Au collisions at $\sqrt{s_{NN}} = 54.4$ GeV. We also observe a difference in v_n between baryon and anti-baryon which is discussed separately in a later section. The high precision measurements of v_n for K_S^0 , ϕ , Λ , Ξ , and Ω presented in this paper can be used to constrain various models, for example, in extracting transport properties of the medium created at $\sqrt{s_{NN}} = 54.4$ GeV.

B. Centrality dependence of v_2 and v_3

The centrality dependence of v_2 and v_3 of K_S^0 , ϕ , Λ , Ξ^- , Ω^- (and their anti-particles) are studied. Figures 5 and 6 show v_2 and v_3 , respectively, as a function of p_T for three different centrality classes, 0-10%, 10-40% and 40-80%. For ϕ , Ξ and Ω measurements are only possible for v_3 for the 0-10% and 10-40% centralities due to data sample size. We observe a strong centrality dependence of v_2 for all the particles, with the magnitude increasing from central to peripheral collisions. This is expected if v_2 is driven by the shape of the initial overlap of the two colliding nuclei [30].

We observe a weak centrality dependence for v_3 compared to v_2 . This observation is consistent with the scenario in which v_3 mostly originates from event-by-event fluctuations of participant nucleon distributions [40], instead of the impact parameter dominated average participant anisotropy distributions. Our measurements demonstrate that such scenario also works well for 54.4 GeV Au+Au collisions.

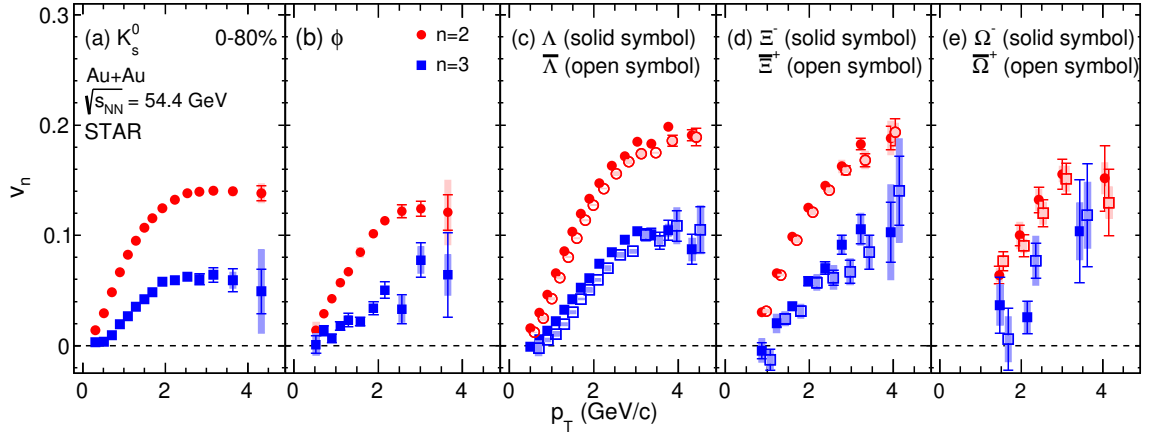


FIG. 4. v_2 and v_3 as a function of p_T at mid-rapidity ($|y| < 1$) for minimum bias events. The vertical lines represent the statistical error bars and the shaded bands represent the systematic uncertainties. Data points for anti-particles are shifted by 0.1 GeV/c towards right for better visibility.

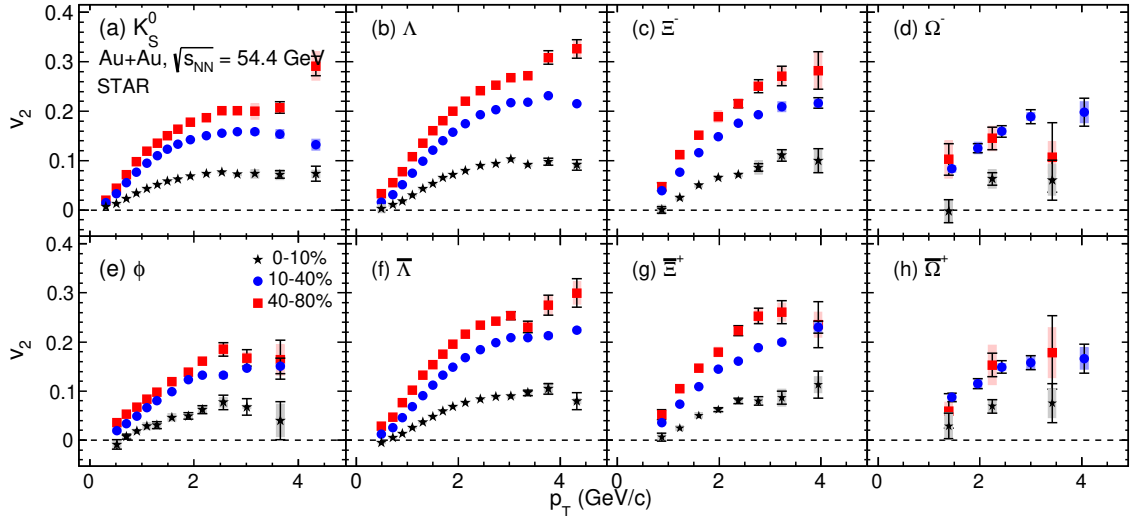


FIG. 5. v_2 as function of p_T for 0-10%, 10-40% and 40-80% centrality events. The vertical lines represent the statistical error bars and the shaded bands represent the systematic uncertainties.

C. Energy dependence of v_2 and v_3

406 The high statistics data at 54.4 GeV from the STAR
 407 experiment offer an opportunity to study the collision
 408 energy dependence of v_2 and v_3 of strange hadrons. Fig-
 409 ure 7 upper panels show v_2 of K_S^0 , ϕ , $\bar{\Lambda}$, $\bar{\Xi}^+$, and Ω^- as
 410 a function of p_T in 0-80% centrality at $\sqrt{s_{NN}} = 39$, 54.4,
 411 and 200 GeV. Lower panels show the ratios with polyno-
 412 mial fits to the 200 GeV data points. K_S^0 v_2 at 54.4 GeV
 413 is smaller than at 200 GeV, and higher than at 39 GeV.
 414 The maximum difference is at intermediate p_T . For $\bar{\Lambda}$
 415 and $\bar{\Xi}^+$, v_2 at 54.4 GeV (as well as at 39 GeV) is higher
 416 than at 200 GeV at very low p_T . This could be due to the
 417 effect of large radial flow at 200 GeV compared to 54.4
 418 and 39 GeV. This effect is only visible in heavier hadrons
 419 like $\bar{\Lambda}$ and $\bar{\Xi}^+$. For ϕ and Ω^- , statistical errors at low

420 p_T are too large to draw any conclusions. Figure 8 upper
 422 panels shows v_3 of K_S^0 , ϕ , and $\bar{\Lambda}$ as a function of p_T in
 423 0-80% centrality at $\sqrt{s_{NN}} = 54.4$, and 200 GeV. Lower
 424 panels show the ratios of fits to the 200 GeV data points.
 425 We observe that the difference in v_3 between 54.4 and
 426 200 GeV is almost p_T independent for all the particles
 427 studied. In Fig. 8, the v_3 shows greater variation as a
 428 function of beam energy than that of v_2 . The measured
 429 ratio of $v_3(54.4 \text{ GeV})/v_3(200 \text{ GeV})$ for K_S^0 is ~ 0.8 while
 430 the same ratio for v_2 is approaching 0.9. This suggests
 431 that the dynamics responsible for v_3 , presumably fluc-
 432 tuations dominated, are more sensitive to beam energy
 433 than the v_2 .

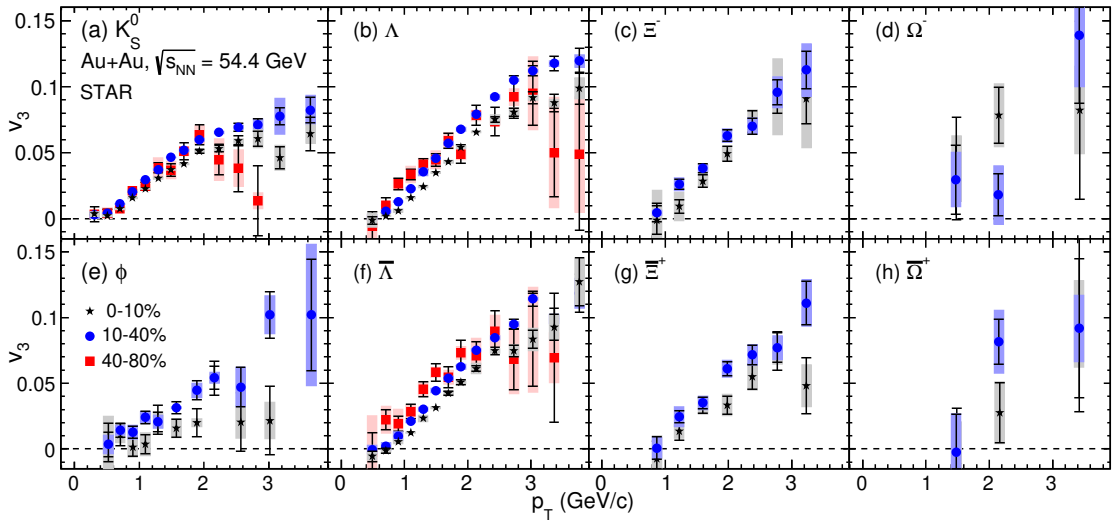


FIG. 6. v_3 as function of p_T for 0-10%, 10-40% and 40-80% centrality events. The vertical lines represent the statistical error bars and the shaded bands represent the systematic uncertainties. 40-80% centrality data points are not shown for Ξ and Ω due to less statistics.

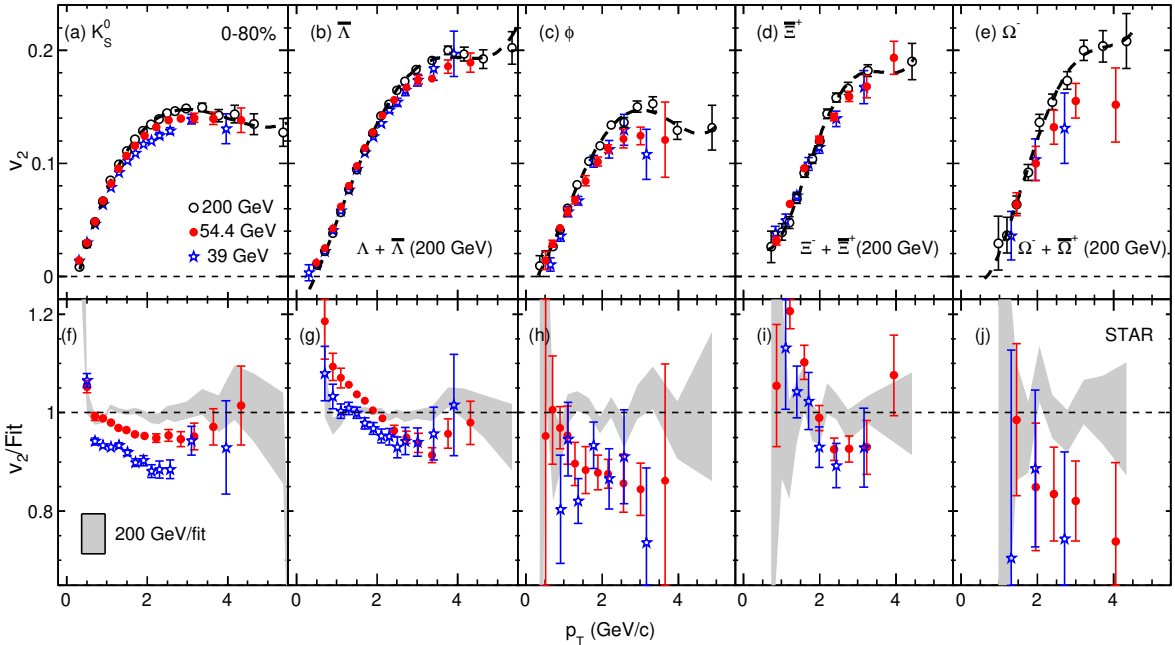


FIG. 7. v_2 of K_S^0 , ϕ , $\bar{\Lambda}$, $\bar{\Xi}^+$, and Ω^- as a function of p_T in 0-80% centrality events at $\sqrt{s_{NN}} = 39, 54.4,$ and 200 GeV. The dotted line represents the fit to the 200 GeV data points. The vertical lines represent the sum of statistical and systematic uncertainties in quadrature. The data points for 39 and 200 GeV are taken from refs. [18, 20, 42]

D. v_n of particles and anti-particles

435 In the upper panels Fig 9, we show the ratio of v_2
 436 and v_3 of particles ($v_n(X)$) to the corresponding anti-
 437 particles ($v_n(\bar{X})$) for Λ , Ξ , and Ω in 10-40% centrality
 438 as a function of p_T . We also present the difference be-
 439 tween v_2 and v_3 of particles and anti-particles in the lower
 440 panels of Fig. 9. We can not establish a clear p_T depen-

441 dence in the ratio or difference of multi-strange parti-
 442 cle and anti-particle. The Λ and $\bar{\Lambda}$ v_n data seem to be
 443 consistent with a relatively smaller v_n for $\bar{\Lambda}$ in the low
 444 p_T region. We have calculated the p_T integrated aver-
 445 age difference in v_n between baryon and anti-baryon by
 446 fitting the $v_n(X) - v_n(\bar{X})$ versus p_T with a zeroth order
 447 polynomial function as done in Ref. [20]. Figure 10
 448 shows the average difference between v_n of baryons and

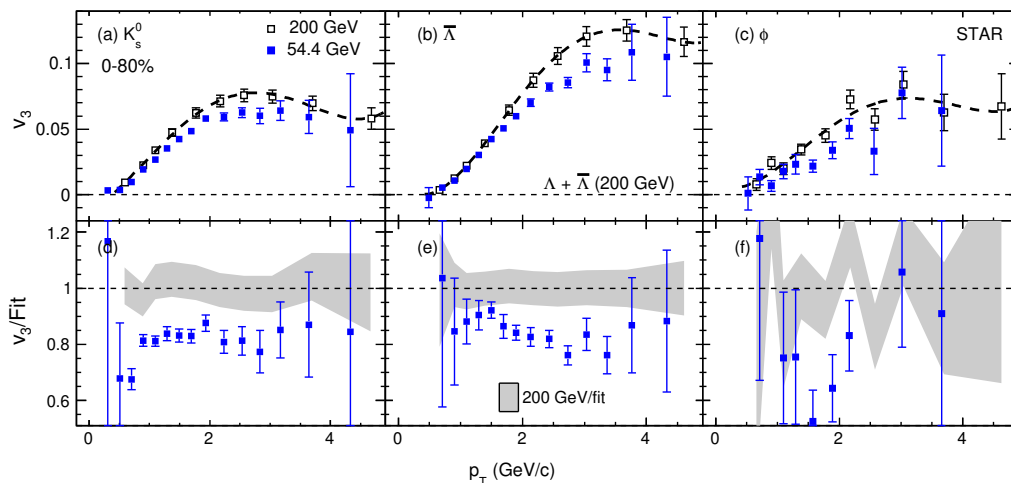


FIG. 8. v_3 of K_S^0 , ϕ and $\bar{\Lambda}$ as a function of p_T in 0-80% centrality events at $\sqrt{s_{\text{NN}}} = 54.4$, and 200 GeV. The vertical lines represent the sum of statistical and systematic uncertainties in quadrature. The data points for 200 GeV are taken from ref. [43].

449 anti-baryons for Λ , Ξ , and Ω in 10-40% centrality as a 450 function of mass. The difference is independent of baryon 451 species within the measured uncertainty for both v_2 and 452 v_3 . The magnitude of the observed difference between 453 particle and anti-particle is similar to that in 62.4 GeV 454 published by the STAR experiment [21]. However, uncer- 455 tainties on the measured values are significantly reduced 456 at 54.4 GeV. The observed difference between particles 457 and anti-particles could arise due to the effect of trans- 458 ported quarks at low beam energies as predicted in [44]. 459 Alternatively, a calculation based on the Nambu-Jona- 460 Lasinio (NJL) model [45, 46] can also qualitatively ex- 461 plain the differences between particles and anti-particles 462 by considering the effect of the vector mean-field poten- 463 tial, which is repulsive for quarks and attractive for anti- 464 quarks. We also measure the difference between Ω^- and 465 $\bar{\Omega}^+$, however the observed difference is not statistically 466 significant ($<1\sigma$ significance).

E. $v_3/v_2^{3/2}$ ratio

468 The ratios between different orders of flow harmonics 469 are predicted to be sensitive probes of transport prop- 470 erties of the produced medium in heavy-ion collisions. 471 According to hydrodynamic model calculations, the ra- 472 tio $v_3/v_2^{3/2}$ is independent of p_T and its magnitude de- 473 pends on the transport properties (e.g., viscosity) of the 474 medium [47–49]. We have calculated the ratio $v_3/v_2^{3/2}$ as 475 a function of p_T for K_S^0 , Λ , Ξ^- , Ω^- , ϕ , $\bar{\Lambda}$, $\bar{\Xi}^+$ and $\bar{\Omega}^+$ for 476 10-40% centrality, as shown in Fig. 11. Our measurement 477 for K_S^0 clearly demonstrates a p_T dependence of the ra- 478 tio. The p_T dependence of the ratios for Λ is weak and 479 ratios for other strange hadrons are limited by statisti- 480 cal errors. Detailed comparisons with other RHIC mea- 481 surements [50, 51] and with more hydrodynamic model

482 calculations will shed more light on the dynamics.

F. Number of constituent quark scaling of v_2 and v_3

484 Elliptic flow measurements at top RHIC energy suggest 485 that a strongly-interacting partonic matter is produced 486 in Au+Au collisions [18]. This conclusion is based in 487 part on the observation that the elliptic flow for identi- 488 fied baryons and mesons when divided by the number of 489 constituent quarks (n_q) is found to scale with the trans- 490 verse kinetic energy of the particles.

491 Figure 12(a) and (b) show the v_2/n_q as a function 492 of n_q scaled transverse kinetic energy in 10-40% central 493 Au+Au collisions at $\sqrt{s_{\text{NN}}} = 54.4$ GeV. The transverse 494 kinetic energy is $m_T - m_0$ where m_T is the transverse 495 mass given by $m_T = \sqrt{m_0^2 + p_T^2}$ and m_0 is the rest mass 496 of the particle. Due to the observed difference in parti- 497 cle and anti-particle v_n we plot v_2/n_q vs. $(m_T - m_0)/n_q$ 498 for particle and anti-particle separately. The n_q -scaled 499 v_2 for identified hadrons including multi-strange hadrons 500 are found to scale with the scaled kinetic energy of the 501 particles. To quantify the validity of scaling we have fit- 502 ted the scaled v_2 of K_S^0 with a 4th order polynomial, 503 and ratios to the fit for different particles have shown in 504 lower panels of Fig. 12. It is found that the scaling holds 505 within a maximum deviation of 10% for all the parti- 506 cles. The observed scaling in v_2 can be interpreted as 507 due to the development of substantial collectivity in the 508 partonic phase [52] and as evidence that coalescence is 509 the dominant mechanism of particle production for the 510 intermediate p_T range.

511 The scaling properties in v_3 have also been examined 512 by plotting $v_3/(n_q)^{3/2}$ as a function of $(m_T - m_0)/n_q$ as 513 shown in panels (a) and (b) of Fig. 13. From the ratios 514 shown in the lower panels, we note that the scaling of 515 $v_3/(n_q)^{3/2}$ is clearly violated for Λ particles and the sta-

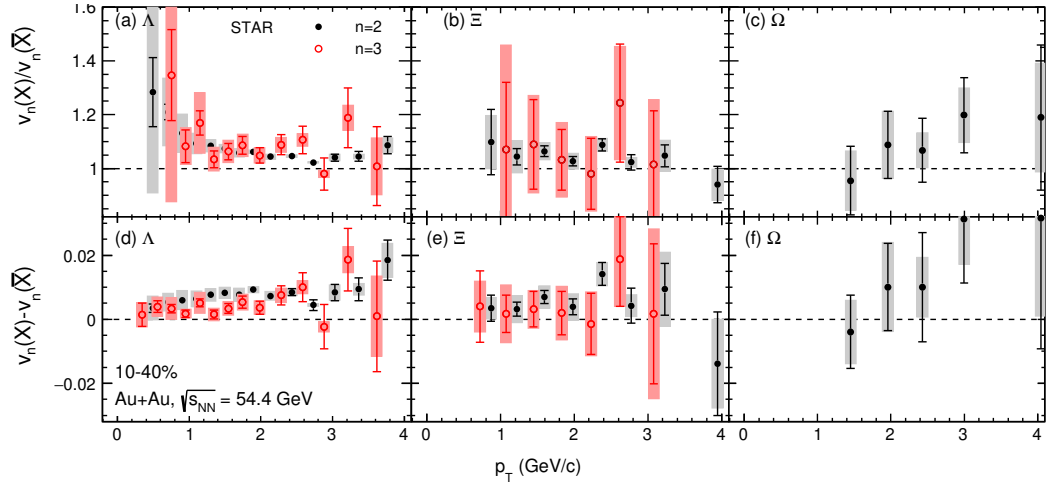


FIG. 9. Three upper panels, a, b, and c show the ratio of v_n of particles to anti-particles for Λ , Ξ and Ω respectively in 10-40% centrality. The lower panels show the difference between v_n of particles to anti-particles. The vertical lines represent the statistical error bars and the shaded bands represent the systematic uncertainties. Data points for v_3 are shifted by 0.15 GeV/c towards the left for better visibility. For the Ω , data points for v_3 were not shown due to fewer statistics.

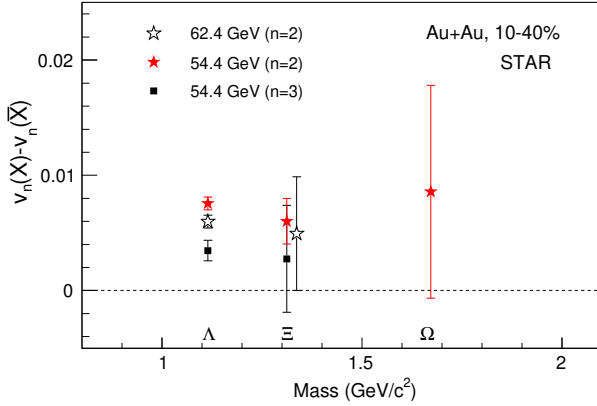


FIG. 10. The difference of v_n of particles and anti-particles is plotted as a function of mass. The result is compared with 62.4 GeV. Uncertainties represent the sum of statistical and systematic in quadrature.

516 tistical errors for multi-strange particles are too large to
517 draw a conclusion regarding scaling.

518 G. $v_2(\phi)/v_2(\bar{p})$ ratio

519 Among many mesons, the $\phi(s\bar{s})$ has unique properties.
520 It has a mass of $1.019 \text{ GeV}/c^2$ which is comparable to the
521 mass of the lightest baryon, the proton ($0.938 \text{ GeV}/c^2$).
522 A hydrodynamical inspired study of transverse momen-
523 tum distribution of ϕ meson seems to suggest that it
524 freezes out early compared to other hadrons such as the
525 proton [2]. Therefore, the kinematic properties of ϕ are
526 expected to be less affected by the later stage hadronic
527 interactions compared to the proton.
528 Hydrodynamical model calculations predict that v_2 of

529 identified hadrons as a function of p_T will follow mass
530 ordering, where the v_2 of lighter hadrons is higher than
531 that of heavier hadrons. A phenomenological calcula-
532 tion [53], based on ideal hydrodynamics together with a
533 hadron cascade (JAM), shows that because of late-stage
534 hadronic rescattering effects on the proton, the mass or-
535 dering in v_2 will be violated between ϕ and proton at
536 very low p_T . This model calculation was done by assum-
537 ing a small hadronic interaction cross-section for the ϕ
538 meson and a larger hadronic interaction cross-section for
539 protons, which is likely true for scatterings off the most
540 abundant pions in the final state. However, several exper-
541 imental and theoretical works on the ϕ -nucleon interac-
542 tion that suggest that the magnitude of the cross section
543 may not be negligible and more quantitative evaluations
544 will be needed [54–62].

545 The breaking of mass ordering in v_2 between ϕ and pro-
546 ton was observed in central Au+Au collisions at $\sqrt{s_{NN}}$
547 = 200 GeV and reported by the STAR experiment in
548 Ref. [18]. Figure 14(a) shows $v_2(\phi)/v_2(\bar{p})$ vs. p_T for
549 10-40% and 40-80% centralities at $\sqrt{s_{NN}} = 54.4 \text{ GeV}$.
550 The result for 0-10% is not shown due to very large un-
551 certainties. Anti-protons, which consist of all produced
552 quarks ($\bar{u}\bar{u}\bar{d}$), are used instead of protons to avoid the
553 effect of transported quarks. At $p_T = 0.5 \text{ GeV}/c$, the
554 ratio is greater than one with 1σ significance in 10-40%
555 centrality. In addition, $v_2(\phi)/v_2(\bar{p})$ ratios in 10-40%
556 central collisions are found to be systematically higher than
557 in peripheral 40-80% events. This observed centrality
558 dependence is consistent with the scenario of significant
559 hadronic rescattering effect on v_2 of \bar{p} while the effect for
560 ϕ is considerably smaller [22, 63]. Comparison of the
561 ratios for 0-80% collision centrality from $\sqrt{s_{NN}} = 54.4 \text{ GeV}$
562 and 200 GeV shows consistency with each other within
563 uncertainties for $p_T < 1.0 \text{ GeV}/c$.

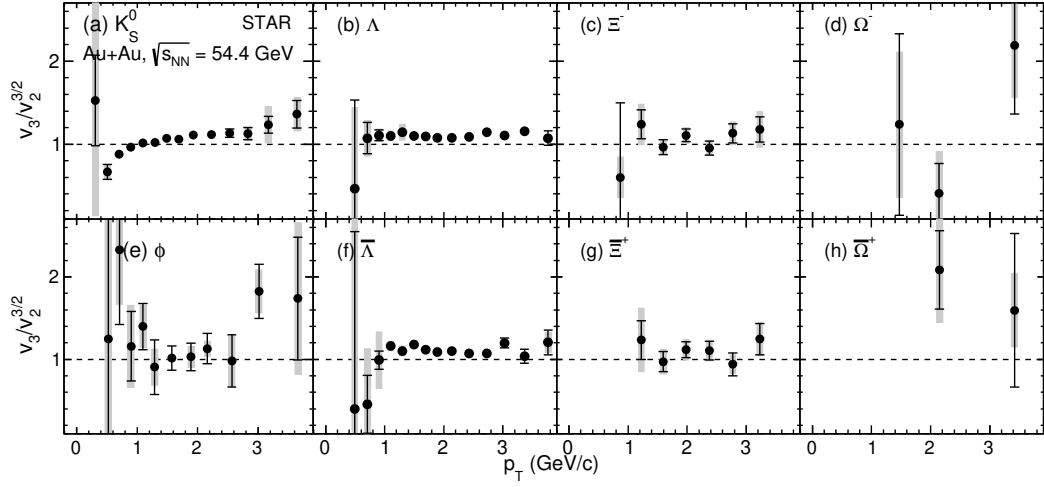


FIG. 11. $v_3/v_2^{3/2}$ is plotted as a function of p_T for K_S^0 , Λ , Ξ^- , Ω^- , ϕ , $\bar{\Lambda}$, $\bar{\Xi}^+$ and $\bar{\Omega}^+$ in 10-40% central Au+Au collisions at $\sqrt{s_{NN}} = 54.4$ GeV.

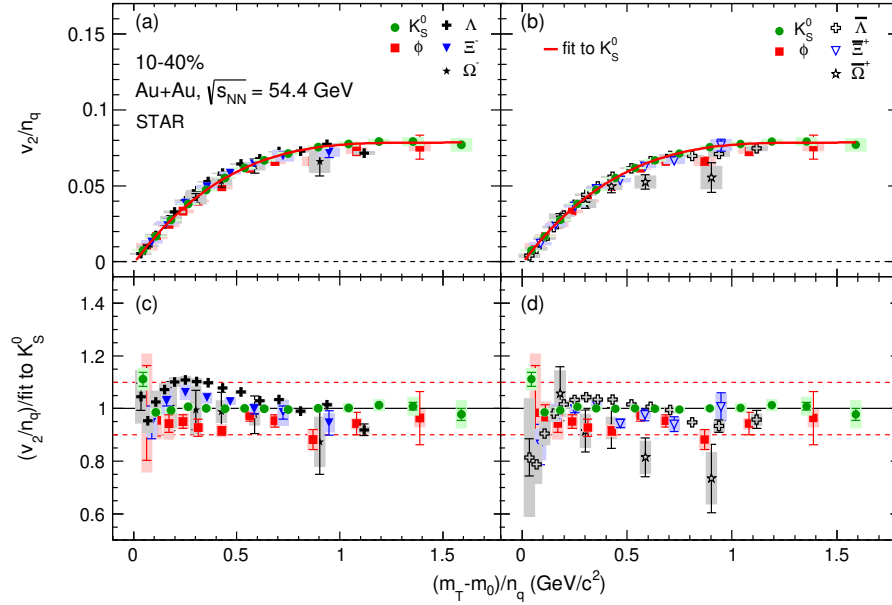


FIG. 12. Panel (a) shows the n_q -scaled v_2 as a function of n_q -scaled transverse kinetic energy for K_S^0 , ϕ , Λ , Ξ^- and Ω^- in 10-40% centrality class events. Panel (b) shows the same for K_S^0 , ϕ , $\bar{\Lambda}$, $\bar{\Xi}^+$ and $\bar{\Omega}^+$. The red line shows the polynomial fit to the K_S^0 data points. Panels (c) and (d) show the ratio of n_q -scaled v_2 of all the particles to the fit function.

564

VI. SUMMARY

565 In summary, we have reported the azimuthal
 566 anisotropic flow parameters, v_2 and v_3 , of strange and
 567 multi-strange hadrons, K_S^0 , ϕ , Λ , Ξ^- , Ω^- (and their anti-
 568 particles) measured at mid-rapidity as a function of p_T
 569 for various collision centralities in Au+Au collisions at
 570 $\sqrt{s_{NN}} = 54.4$ GeV. The magnitude of v_3 of multi-strange
 571 baryons Ξ and Ω is found to be similar to that of the
 572 lighter strange baryon Λ . The non-zero magnitude of v_3
 573 indicates the presence of event-by-event fluctuations in
 574 the initial energy density profile of colliding nuclei and

575 large values of v_2 and v_3 of multi-strange hadrons indi-
 576 cate that the observed collectivity is mainly developed
 577 through partonic rather than hadronic interactions.

578 The centrality dependence of v_3 is weak relative to
 579 that of v_2 which is consistent with the scenario that v_3
 580 does not arise from impact parameter driven average spa-
 581 tial configurations, rather it originates dominantly from
 582 event-by-event fluctuation present in the system. The
 583 measured v_2 and v_3 values at $\sqrt{s_{NN}} = 54.4$ GeV are also
 584 compared with available published results in Au+Au col-
 585 lisions at $\sqrt{s_{NN}} = 39$ and 200 GeV to examine the energy
 586 dependence. We observed that the change in v_3 with

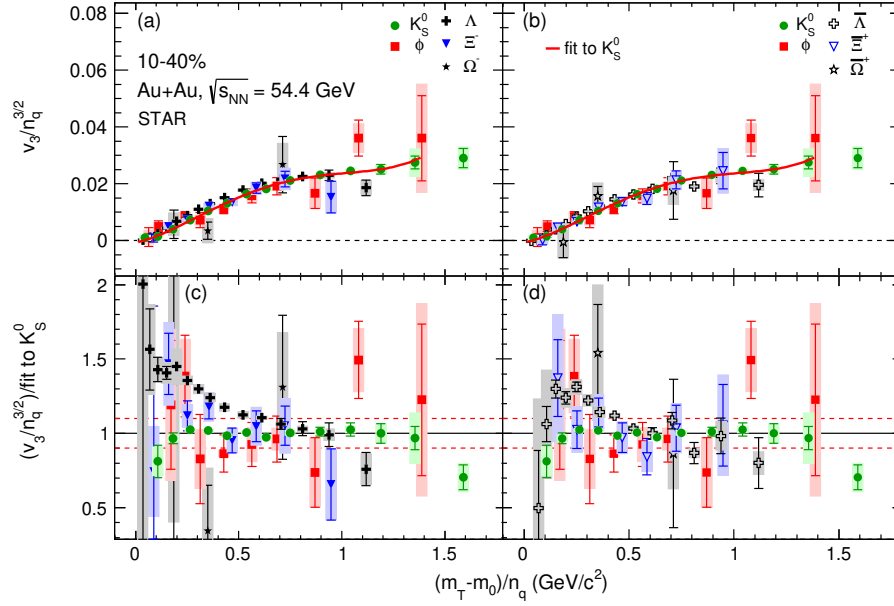


FIG. 13. Panel (a) shows $v_3/n_q^{3/2}$ as a function of n_q -scaled transverse kinetic energy for K_S^0 , ϕ , Λ , Ξ^- and Ω^- in 10-40% centrality class events. Panel (b) shows the same for K_S^0 , ϕ , $\bar{\Lambda}$, Ξ^+ and Ω^+ . The red line shows the polynomial fit to the K_S^0 data points. Panels (c) and (d) show the ratio of $v_3/n_q^{3/2}$ of all the particles to the fit function.

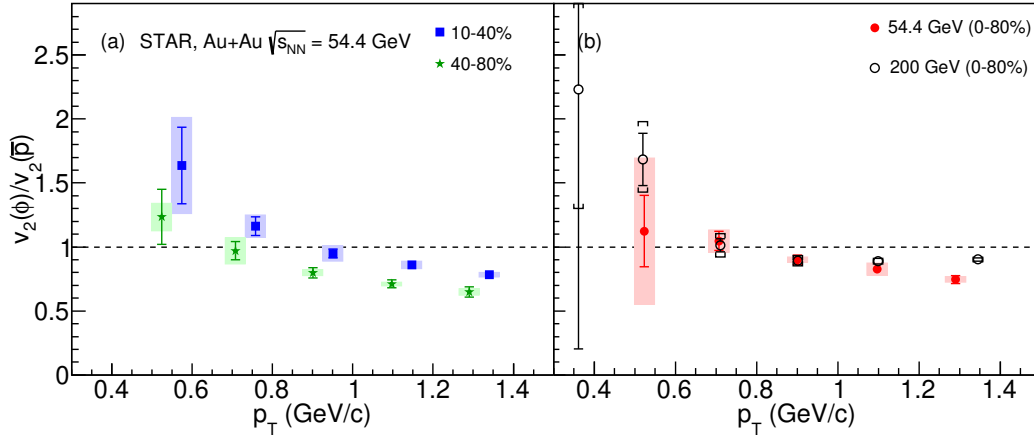


FIG. 14. Left panel shows the ratio of v_2 of ϕ to v_2 of \bar{p} as a function of p_T for 10-40% and 40-80% centralities at $\sqrt{s_{NN}} = 54.4$ GeV. Data points for 10-40% centrality are shifted by 0.05 GeV/c to the right for better visibility. The right panel shows the comparison of the ratio at $\sqrt{s_{NN}} = 54.4$ GeV and 200 GeV in 0-80% centrality. For 200 GeV [18], the measured ratio is $v_2(\phi)/v_2(p + \bar{p})$. The vertical lines represent the statistical error bars and the shaded bands represent the systematic uncertainties. Data points at 200 GeV are taken from ref. [18]

587 $\sqrt{s_{NN}}$ is more than that in v_2 . This suggests that v_3 dynamics have stronger energy dependence compared to v_2 .
 588
 589 A difference in $v_n(p_T)$ between baryons and corresponding antibaryons was observed. The observed difference is
 590
 591 found to be baryon-type independent within uncertainties.
 592

593 We have studied the n_q scaling for both v_2 and v_3
 594 and found that the scaling holds for v_2 of all the particles while the scaling for v_3 seems to be violated. One
 595
 596 interpretation of the observed n_q scaling in v_2 is that

597 parton recombination is the dominant mechanism for
 598 hadronization at mid-rapidity and the development of
 599 collectivity occurs during the partonic stage of the system evolution. The ratio $v_3/v_2^{3/2}$, which is sensitive to
 600 the medium properties according to hydrodynamic calculations, shows weak p_T dependence for $p_T > 1$ GeV/c,
 601 similar to the behaviour of this ratio was found in the
 602 previous study with U+U collisions at 193 GeV. The
 603
 604 $v_2(\phi)/v_2(\bar{p})$ ratio was presented as a function of p_T for
 605 two different centrality classes 10-40% and 40-80%. The
 606

607 $v_2(\phi)/v_2(\bar{p})$ ratio shows a decreasing trend as a function
 608 of p_T for both collision centralities. The $v_2(\phi)/v_2(\bar{p})$ ratio
 609 is also found to be systematically higher for central col-
 610 lisions 10-40% than non-central collisions 40-80%. This
 611 could be due the effect of more hadronic rescattering on
 612 v_2 of \bar{p} compared to ϕ and hence our measurements are
 613 consistent with the picture of smaller hadronic rescatter-
 614 ing and earlier freeze out of the ϕ mesons.

615 ACKNOWLEDGMENTS

616 We thank the RHIC Operations Group and RCF at
 617 BNL, the NERSC Center at LBNL, and the Open Science
 618 Grid consortium for providing resources and support.
 619 This work was supported in part by the Office of Nu-
 620 clear Physics within the U.S. DOE Office of Science, the
 621 U.S. National Science Foundation, National Natural Sci-

ence Foundation of China, Chinese Academy of Science,
 623 the Ministry of Science and Technology of China and
 624 the Chinese Ministry of Education, the Higher Education
 625 Sprout Project by Ministry of Education at NCKU, the
 626 National Research Foundation of Korea, Czech Science
 627 Foundation and Ministry of Education, Youth and Sports
 628 of the Czech Republic, Hungarian National Research, De-
 629 velopment and Innovation Office, New National Excel-
 630 lency Programme of the Hungarian Ministry of Human
 631 Capacities, Department of Atomic Energy and Depart-
 632 ment of Science and Technology of the Government of
 633 India, the National Science Centre and WUT ID-UB of
 634 Poland, the Ministry of Science, Education and Sports
 635 of the Republic of Croatia, German Bundesministerium
 636 für Bildung, Wissenschaft, Forschung und Technologie
 637 (BMBF), Helmholtz Association, Ministry of Education,
 638 Culture, Sports, Science, and Technology (MEXT) and
 639 Japan Society for the Promotion of Science (JSPS).

-
- 640 [1] D. J. Gross, R. D. Pisarski, and L. G. Yaffe, Rev. Mod. 680
 641 Phys. 53, 43 (1981).
 642 [2] J. Adams *et al.*, (STAR Collaboration) Nucl. Phys. A757, 681
 643 102 (2005).
 644 [3] K. H. Ackermann *et al.*, (STAR Collaboration), Phys. 682
 645 Rev. Lett. 86, 402 (2001).
 646 [4] J. Adams *et al.*, (STAR Collaboration), Phys. Rev. Lett. 683
 647 92, 052302 (2004).
 648 [5] J. Adams *et al.*, (STAR Collaboration), Phys. Rev. C 72, 684
 649 014904 (2005).
 650 [6] B. I. Abelev *et al.*, (STAR Collaboration), Phys. Rev. 685
 651 Lett. 99, 112301 (2007).
 652 [7] S. S. Adler *et al.*, (PHENIX Collaboration), Phys. Rev. 686
 653 Lett. 91, 182301 (2003).
 654 [8] S. S. Adler *et al.*, (PHENIX Collaboration), Phys. Rev. 687
 655 Lett. 94, 232302 (2005).
 656 [9] B. Alver *et al.* (PHOBOS Collaboration), Phys. Rev. 688
 657 Lett. 98, 242302 (2007).
 658 [10] J. Y. Ollitrault, Phys. Rev. D 46, 229 (1992).
 659 [11] P. Huovinen, P. F. Kolb, U. Heinz, P. V. Ruuskanen, and 689
 660 S.A. Voloshin *et al.*, Phys. Lett. B 503, 58 (2001).
 661 [12] C. Shen and U. Heinz, Phys. Rev. C 85, 054902 (2012).
 662 [13] R. Snellings, New J. Phys. 13, 055008 (2011).
 663 [14] H. Appelshauser *et al.*, (NA49 Collaboration), Phys. Rev. 690
 664 Lett. 80, 4136 (1998).
 665 [15] K. Aamodt *et al.*, (ALICE Collaboration), Phys. Rev. 691
 666 Lett. 105, 252302 (2010).
 667 [16] G. Aad *et al.*, (ATLAS Collaboration), Phys. Lett. B 707, 692
 668 330 (2012).
 669 [17] S. Chatrchyan *et al.* (CMS Collaboration), Phys. Rev. C 693
 670 89, 044906 (2014).
 671 [18] L. Adamczyk *et al.*, (STAR Collaboration), Phys. Rev. 694
 672 Lett. 116, 062301 (2016).
 673 [19] M.M. Aggarwal *et al.*, (STAR Collaboration), Phys. Rev. 695
 674 Lett. 110, 142301 (2013).
 675 [20] L. Adamczyk *et al.*, (STAR Collaboration) Phys. Rev. 696
 676 Lett. 110, 142301 (2013).
 677 [21] L. Adamczyk *et al.*, (STAR Collaboration) Phys. Rev. C 697
 678 88, 014902 (2013).
 679 [22] A. Shor, Phys. Rev. Lett. 54, 1122 (1985).
 680 [23] X. Luo, et al. Particles 3, no.2, 278 (2020).
 681 [24] B. Mohanty and N. Xu, J. Phys. G 36, 064022 (2009).
 682 [25] J.H. Chen, et al., Phys. Rev. C 74, 064902 (2006).
 683 [26] M. Nasim, B. Mohanty, and N. Xu, Phys. Rev. C 87, 684
 685 014903 (2013).
 686 [27] J. Adam *et al.*, (ALICE Collaboration), Eur. Phys. J. C 685
 686 76, 245 (2016).
 687 [28] K.H. Ackermann et al., Nucl. Instrum. Methods Phys. 687
 688 Res., Sect. A 499, 624 (2003).
 689 [29] R. J. Glauber, Nucl. Phys. A 774, 3 (2006).
 690 [30] L. Adamczyk *et al.*, (STAR Collaboration) Phys. Rev. C 690
 691 86, 054908 (2012).
 692 [31] W. J. Llope (STAR TOF Group), Nucl. Instrum. Meth- 691
 693 ods Phys.Res., Sect. B 241, 306 (2005).
 694 [32] D. Drijard, H.G. Fischer and T. Nakada, Nucl. Inst. 692
 695 Meth. in Phys. Res. A 225, 367 (1984).
 696 [33] J. Adams *et al.*, (STAR Collaboration) Phys. Rev. Lett. 693
 694 95, 122301 (2005).
 695 [34] C. Adler *et al.*, (STAR Collaboration) Phys. Rev. Lett. 694
 696 89, 132301 (2002).
 697 [35] M. S. Abdallah *et al.*, (STAR Collaboration) Phys. Rev. 695
 698 C 103, 064907, (2021).
 699 [36] A. M. Poskanzer and S. A. Voloshin, Phys. Rev. C 58, 700
 700 1671 (1998).
 701 [37] H. Masui, A. Schmah, A. M. Poskanzer, Nucl. Instrum. 701
 702 Meth. A833, 181 (2016).
 703 [38] N. Borghini and J.-Y. Ollitrault, Phys. Rev. C 70, 064905 702
 704 (2004).
 705 [39] R. Barlow, arXiv:hep-ex/0207026.
 706 [40] B. Alver and G. Roland, Phys. Rev. C 81, 054905 (2010); 703
 707 82, 039903(E) (2010);
 708 [41] M. Luzum, P. Romatschke, Phys. Rev. C 78, 034915 704
 709 (2008).
 710 [42] B. I. Abelev *et al.*, (STAR Collaboration) Phys. Rev. C 705
 711 77, 054901 (2008).
 712 [43] M. S. Abdallah *et al.*, (STAR Collaboration) arXiv:nuc- 706
 713 lex/2203.07204
 714 [44] J. C. Dunlop, M. A. Lisa, and P. Sorensen, Phys. Rev. C 707
 715 84, 044914 (2011).
 716 [45] C. M. Ko *et al.*, Nucl. Phys. A 928, 234 (2014). 708

- 720 [46] Jun Xu, Taesoo Song, Che Ming Ko, and Feng Li, Phys. 735 [55] A. Polyanskiy *et al.*, Phys. Lett. B 695, 74 (2011).
721 Rev. Lett. 112, 012301 (2014). 736 [56] S. Acharya *et al.*, (ALICE Collaboration) Phys. Rev.
722 [47] E. Retinskaya, M. Luzum, and J.-Y. Ollitrault, 737 Lett. 127, 172301 (2021).
723 Phys.Rev. C 89, 014902 (2014). 738 [57] R. Muto *et al.*,(KEK-PS-E325 Collaboration), Phys.
724 [48] E. Retinskaya, M. Luzum, and J.-Y. Ollitrault, Nucl. 739 Rev. Lett. 98, 042501 (2007).
725 Phys. A 926, 152 (2014). 740 [58] M. Wood *et al.*, (CLAS Collaboration), Phys. Rev. Lett.
726 [49] C. Lang and N. Borghini, Eur.Phys.J. C 74, 2955 (2014). 741 105, 112301 (2010).
727 [50] J. Adams *et al.*, (STAR Collaboration), Phys. Rev. Lett. 742 [59] J. Adamczewski-Musch *et al.*, (HADES Collaboration),
728 92, 062301 (2004). 743 Phys. Rev. Lett. 123, 022002 (2019).
729 [51] A. Adare *et al.*, (PHENIX Collaboration), Phys. Rev. 744 [60] S. Leupold *et al.*, Int. J. Mod. Phys. E 19, 147 (2010).
730 Lett. 105, 062301 (2010). 745 [61] D. Cabrera *et al.*, Phys. Rev. C 96, 034618 (2017).
731 [52] D. Molnar and S. A. Voloshin, Phys. Rev. Lett. 91, 092301 746 [62] Y. Koike and A. Hayashigaki, Prog. Theor. Phys. 98, 631
732 (2003). 747 (1997).
733 [53] T. Hirano and Y. Nara, Phys. Rev. C 69, 034908 (2004). 748 [63] H. van Hecke *et al.*, Phys. Rev. Lett. 81, 5764 (1998).
734 [54] A. Sibirtsev *et al.*, Eur. Phys. J. A 37, 287301 (2008).